JOURNAL OF GEOPHYSICAL RESEARCH, VOL. 113, A07301, doi:10.1029/2007JA012918, 2008

Theoretical models of ionospheric electrodynamics and plasma transport

Paul Withers[1]

Received 1 November 2007; revised 5 March 2008; accepted 17 March 2008; published 3 July 2008.

[1] A relationship between $\underline{J}$, the current density, and $\underline{E}'$, the electric field measured in the frame of the neutral wind, is derived for a planetary ionosphere: $\underline{J} = \underline{Q} + \underline{\underline{S}}\,\underline{E}'$. If pressure gradients and gravity are neglected, this reduces to the well-known $\underline{J} = \underline{\underline{\sigma}}\,\underline{E}'$, where $\underline{\underline{\sigma}}$ is the conductivity tensor. If $\underline{J} = 0$, this reduces to ambipolar diffusion. Neither $\underline{J} = \underline{\underline{\sigma}}\,\underline{E}'$ nor ambipolar diffusion can describe the vertical motion of plasma in a dynamo region, a region where electrons are tied to fieldlines, but ions are not. This has prevented models from accurately describing how vertical plasma transport affects plasma densities in the martian ionosphere. The relationship $\underline{J} = \underline{Q} + \underline{\underline{S}}\,\underline{E}'$ is applied to a one-dimensional ionospheric model to study ion velocities, electron velocities, currents, electric fields, and induced magnetic fields simultaneously and self-consistently. In this model, ion and electron velocities transition smoothly from moving across fieldlines below the dynamo region to moving along fieldlines above the dynamo region. This relationship is valid for the terrestrial ionosphere; replacing $\underline{J} = \underline{\underline{\sigma}}\,\underline{E}'$ with $\underline{J} = \underline{Q} + \underline{\underline{S}}\,\underline{E}'$ in terrestrial models may alter some of their predictions.

Citation: Withers, P. (2008), Theoretical models of ionospheric electrodynamics and plasma transport, *J. Geophys. Res.*, *113*, A07301, doi:10.1029/2007JA012918.

1. Introduction

[2] Moving charged particles are accelerated by magnetic fields. If the effects of magnetic fields are stronger than the effects of collisions and other forces, then charged particles cannot cross magnetic fieldlines [*Rishbeth and Garriott*, 1969; *Kelley*, 1989]. In the mid-latitude terrestrial ionosphere, electrons and ions are ''frozen-in'' to fieldlines above 75 km and 130 km, respectively [*Rishbeth and Garriott*, 1969]. The intermediate region between 75 and 130 km is known as the dynamo region, within which currents flow.

[3] An ionospheric model must have a realistic representation of the electric field, which also accelerates charged particles, if it is to describe the motion of ionospheric plasma accurately. Empirical electric field models that are based on direct observations exist only for Earth [e.g., *Richmond et al.*, 1980]. Theoretical approaches to determining the electric field include ambipolar diffusion and the conductivity equation. Ambipolar diffusion, which assumes that no current flows through the ionosphere, can predict the electric field below the dynamo region, but not within the dynamo region [*Rishbeth and Garriott*, 1969]. The conductivity equation, which assumes that the effects of gravity and pressure gradients on charged particles are negligible, can predict the electric field in an ionosphere, but its assumptions fail where plasma motion is not horizontal [*Forbes*, 1981]. Therefore existing theory offers only an incomplete description of the vertical motion of plasma in a dynamo region [e.g., *Forbes*, 1981; *Richmond*, 1983; *Kelley*, 1989].

[4] This is not generally considered a problem for terrestrial ionospheric studies because plasma transport has a negligible effect on plasma densities in the dynamo region [*Rishbeth and Garriott*, 1969]. Vertical transport of plasma is only important at higher altitudes. The effects of these problems are more obvious on Mars, which has a weak crustal magnetic field. Magnetic field strength and direction vary on lengthscales of hundreds of kilometers, much smaller than the planetary radius [*Acuña et al.*, 1999; *Connerney et al.*, 1999]. Dynamo regions on some parts of Mars occur at altitudes where plasma transport has a significant effect on plasma densities.

[5] In this paper, theoretical tools are developed to determine ionospheric electromagnetic fields and their effects on ion and electron velocities. These tools are more complete than current implementations of ambipolar diffusion and the conductivity equation. These tools are directly applicable to martian ionospheric studies, are a generalization of theories currently applied to the terrestrial ionosphere, and may be useful for terrestrial ionospheric and magnetospheric studies. We focus on general theory in this paper, so specific application of these tools to problems in terrestrial ionospheric studies will be addressed in future work.

[6] We first discuss weaknesses in existing models of ambipolar diffusion (section 2). We then use the conservation of momentum to obtain a relationship between current density and electric field (sections 3–5), explore the constraints imposed by Maxwell's equations (section 6), and show that current implementations of ambipolar diffusion and the conductivity equation are special cases of our more

[1]Center for Space Physics, Boston University, Boston, Massachusetts, USA.

0148-0227/08/2007JA012918$09.00

general formulae (sections 7–8). We finally apply this general theory to a simplified Mars-like ionosphere to demonstrate that it accurately describes the vertical motion of plasma in a dynamo region (sections 9–10).

2. Introduction to Ambipolar Diffusion

[7] We motivate this work by demonstrating that ambipolar diffusion provides an incomplete description of plasma motion. Consider a quasi-neutral ionospheric plasma that has one ionic species, no horizontal gradients, and no atmospheric winds. If ion-electron collisions are neglected, the steady state ion and electron velocities satisfy [*Rishbeth and Garriott*, 1969]:

$$0 = m_i\underline{g} - \frac{1}{N}\underline{\nabla}(NkT_i) + e\underline{E} + e\underline{v_i} \times \underline{B} - m_i\nu_{in}\underline{v_i} \tag{1}$$

$$0 = m_e\underline{g} - \frac{1}{N}\underline{\nabla}(NkT_e) - e\underline{E} - e\underline{v_e} \times \underline{B} - m_e\nu_{en}\underline{v_e} \tag{2}$$

where subscript e refers to electrons and subscript i refers to ions, m is mass, $\underline{g}$ is the acceleration due to gravity, N is ion density, which equals the electron density, k is Boltzmann's constant, T is temperature, $-e$ is the charge on an electron, $\underline{E}$ is the electric field, $\underline{B}$ is the magnetic field, $\underline{v}$ is velocity, ν_{in} is the ion-neutral collision frequency, and ν_{en} is the electron-neutral collision frequency.

[8] A relationship between $v_{i,z}$ and $v_{e,z}$, where the z axis is vertical, can be derived from charge conservation, which requires that:

$$\underline{\nabla} \cdot \underline{J} + \frac{\partial \rho}{\partial t} = 0 \tag{3}$$

where $\underline{J}$ is current density and ρ is charge density. For a quasi-neutral plasma, equation (3) reduces to:

$$\underline{\nabla} \cdot \underline{J} = 0 \tag{4}$$

[9] Since there are no horizontal gradients, equation (4) reduces to:

$$\frac{\partial J_z}{\partial z} = 0 \tag{5}$$

so J_z is uniform. If there is no external current source, then currents cannot flow outside the ionosphere and J_z must be zero. Since $\underline{J}$ is defined as:

$$\underline{J} = eN\left(\underline{v_i} - \underline{v_e}\right) \tag{6}$$

it follows that:

$$v_{i,z} = v_{e,z} = v_z \tag{7}$$

where v_z is defined by equation (7). The vertical components of equations (1) and (2) become:

$$0 = -m_i g - \frac{1}{N}\frac{\partial(NkT_i)}{\partial z} + eE_z + e\left(v_{i,x}B_y - v_{i,y}B_x\right) - m_i\nu_{in}v_z \tag{8}$$

$$0 = -m_e g - \frac{1}{N}\frac{\partial(NkT_e)}{\partial z} - eE_z - e\left(v_{e,x}B_y - v_{e,y}B_x\right) - m_e\nu_{en}v_z \tag{9}$$

[10] If $B_x = 0$ and $B_y = 0$, then the sum of equations (8) and (9) is:

$$0 = -(m_i + m_e)g - \frac{1}{N}\frac{\partial(Nk(T_i + T_e))}{\partial z} - (m_i\nu_{in} + m_e\nu_{en})v_z \tag{10}$$

[11] Since $m_e \ll m_i$ and $m_e\nu_{en} \ll m_i\nu_{in}$, v_z is [*Rishbeth and Garriott*, 1969]:

$$v_A = v_z = \frac{-1}{m_i\nu_{in}}\left(m_i g + \frac{1}{N}\frac{\partial(Nk(T_i + T_e))}{\partial z}\right) \tag{11}$$

where v_A is defined by equation (11). Substituting equation (11) into equation (8) and rearranging gives E_z:

$$E_A = E_z = \frac{-1}{eN}\frac{\partial(NkT_e)}{\partial z} \tag{12}$$

where E_A is defined by equation (12). Even if $B_x \neq 0$ or $B_y \neq 0$, equations (11) and (12) are valid if $\underline{B}$ is very weak. A different solution exists if $\underline{B}$ is very strong and inclined at angle I to the horizontal. From equations (1) and (2), components of $\underline{v_i}$ and $\underline{v_e}$ that are perpendicular to $\underline{B}$ must approach zero in the limit that $B \to \infty$. Plasma can only move along a fieldline, parallel to $\underline{B}$. Equation (4) and $J_z = 0$ on the ionosphere's boundary require that $v_{i,\parallel} = v_{e,\parallel}$. Since gravitational and pressure gradient forces are vertical, the plasma velocity parallel to $\underline{B}$ is $v_A \sin I$. The vertical component of the plasma velocity is $v_A \sin^2 I$. The electric field parallel to $\underline{B}$ is $E_A \sin I$.

[12] $\underline{B}$ is very strong if $\Omega_i/\nu_{in} \gg 1$ and $\Omega_e/\nu_{en} \gg 1$, where $\Omega_i = eB/m_i$ is the ion cyclotron frequency and $\Omega_e = eB/m_e$ is the electron cyclotron frequency. $\underline{B}$ is very weak if $\Omega_i/\nu_{in} \ll 1$ and $\Omega_e/\nu_{en} \ll 1$. Typically $m_e\nu_{en} \ll m_i\nu_{in}$, so $\Omega_i/\nu_{in} \ll \Omega_e/\nu_{en}$. Since ν_{in} and ν_{en} are proportional to neutral number density, which decreases exponentially with altitude, whereas $\underline{B}$ changes more slowly with altitude, the effects of $\underline{B}$ become more significant as altitude increases. In general, conditions in an ionosphere around a magnetized body approach the weak field limit at low altitudes and approach the strong field limit at high altitudes, with an intermediate altitude region where $\underline{B}$ is neither very strong nor very weak. This intermediate region is known as the dynamo region and it lies between 75 and 130 km in the terrestrial dayside mid-latitude ionosphere.

[13] The lower and upper boundaries of a dynamo region are defined to occur where $\Omega_e/\nu_{en} = 1$ and $\Omega_i/\nu_{in} = 1$, respectively. Ionospheric plasma densities are controlled via the continuity equation by a combination of photochemical processes and transport processes. In a typical ionosphere, photochemical processes dominate at low altitudes and transport processes dominate at high altitudes. The position of the photochemical/transport boundary relative to the dynamo region is important. If the photochemical/transport boundary occurs above the dynamo region, as in the terrestrial ionosphere, then the strong field limit of ambipolar diffusion ($v_{i,z} = v_{e,z} = v_A \sin^2 I$) can be used to model

how plasma transport affects plasma densities. If the photochemical/transport boundary does not occurs above the dynamo region, which happens on Mars, existing theories are unable to model how plasma transport affects plasma densities.

3. Conservation of Momentum

[14] We now return to first principles to investigate theories of plasma motion. The momentum equations for each species of charged particle in an ionosphere are [*Chandra*, 1964; *Banks and Kockarts*, 1973]:

$$m_j \frac{\partial \underline{v_j}}{\partial t} + m_j \left(\underline{v_j} \cdot \underline{\nabla}\right) \underline{v_j} = m_j \underline{g} - \frac{1}{N_j} \underline{\nabla}\left(N_j k T_j\right) + q_j \underline{E} + q_j \underline{v_j} \times \underline{B} - m_j \nu_{jn} \left(\underline{v_j} - \underline{u}\right) - m_j \left(\sum_{k \neq j} \nu_{jk} \left(\underline{v_j} - \underline{v_k}\right)\right) \tag{13}$$

where t is time, j is an index referring to a charged species, m_j is the mass of a particle of species j, $\underline{v_j}$ is the velocity of species j, $\underline{g}$ is the acceleration due to gravity, N_j is the number density of species j, k is Boltzmann's constant, T_j is the temperature of species j, q_j is the charge of a particle of species j, $\underline{E}$ is the electric field, $\underline{B}$ is the magnetic field, ν_{jn} is the "diffusion collision frequency" for collisions between particles of species j and neutrals n, $\underline{u}$ is the neutral wind velocity, and ν_{jk} is the "diffusion collision frequency" for collisions between charged particles of species j and k. The current density, $\underline{J}$, is defined as.

$$\underline{J} = \sum_j N_j q_j \underline{v_j} \tag{14}$$

[15] In a planet-fixed frame, $\underline{g}$ includes centrifugal acceleration and any tidal accelerations. Equation (13) neglects viscosity and Coriolis forces. For convenience, $\underline{w_j}$ and $\underline{E}'$ are defined by:

$$\underline{w_j} = \underline{v_j} - \underline{u} \tag{15}$$

$$\underline{E}' = \underline{E} + \underline{u} \times \underline{B} \tag{16}$$

[16] $\underline{E}'$ is the electric field in a frame of reference moving at the neutral wind velocity, $\underline{u}$, and $\underline{w_j}$ is the velocity of species j in that frame [*Kelley*, 1989]. Since the Debye length of typical ionospheric plasmas is much smaller than any characteristic lengthscale of the ionosphere, the plasma must be quasi-neutral [*Kelley*, 1989; *Rishbeth*, 1997]:

$$\sum_j N_j q_j = 0 \tag{17}$$

[17] To simplify the $\underline{v_j} \times \underline{B}$ term in equation (13), B and unit vector $\hat{b}$ are defined by $B\underline{\hat{b}} = \underline{B}$, and $\underline{\underline{\Lambda}}$ is defined by:

$$\underline{X} \times \underline{B} = \underline{\underline{\Lambda}}\, \underline{X} \tag{18}$$

where $\underline{X}$ is any vector. In component form, $\underline{\underline{\Lambda}}$ is:

$$\underline{\underline{\Lambda}} = \begin{pmatrix} 0 & +b_z & -b_y \\ -b_z & 0 & +b_x \\ +b_y & -b_x & 0 \end{pmatrix} \tag{19}$$

[18] $\underline{\underline{\Lambda}}^{-1}$ does not exist. Equation (13) is linearized by neglecting the $(\underline{v_j} \cdot \underline{\nabla})\, \underline{v_j}$ term, $\partial \underline{v_j}/\partial t$ is neglected to enforce steady state conditions, and equations (15)–(18) are used to rearrange equations (13)–(14):

$$0 = m_j \underline{g} - \frac{1}{N_j} \underline{\nabla}\left(N_j k T_j\right) + q_j \underline{E}' + q_j B \underline{\underline{\Lambda}}\, \underline{w_j} - m_j \nu_{jn} \underline{w_j} - m_j \left(\sum_{k \neq j} \nu_{jk} \left(\underline{w_j} - \underline{w_k}\right)\right) \tag{20}$$

$$\underline{J} = \sum_j N_j q_j \underline{w_j} \tag{21}$$

[19] Suppose all quantities in equations (20) and (21), except $\underline{J}$, $\underline{E}'$, and $\underline{w_j}$, are known. If there are p species of ions, then equations (20) and (21) provide $p + 2$ linear equations linking the $p + 3$ unknowns $\underline{J}$, $\underline{E}'$, and $\underline{w_j}$. Hence these equations *must* lead to a linear relationship between any pair of $\underline{J}$, $\underline{E}'$, and $\underline{w_j}$, such as $\underline{J} = \underline{Q} + \underline{\underline{S}}\, \underline{E}'$.

4. Finding a Linear Relationship Between $\underline{J}$ and $\underline{E}'$

[20] The most general relationship between J and $\underline{E}'$ that is possible is $\underline{J} = \underline{Q} + \underline{\underline{S}}\, \underline{E}'$. Expressions for $\underline{Q}$ and $\underline{\underline{S}}$ are derived in this section after the effects of collisions between charged particles are neglected. Similar methods can be used to obtain more general expressions for $\underline{Q}$ and $\underline{\underline{S}}$ without neglecting these effects. This simplified case is presented to illuminate the underlying physics more clearly. Setting $\nu_{jk} = 0$, equation (20) becomes:

$$0 = m_j \underline{g} - \frac{1}{N_j} \underline{\nabla}\left(N_j k T_j\right) + q_j \underline{E}' + q_j B \underline{\underline{\Lambda}}\, \underline{w_j} - m_j \nu_{jn} \underline{w_j} \tag{22}$$

[21] Rearranging leads to:

$$\underline{w_j} = \left(m_j \nu_{jn} \underline{\underline{I}} - q_j B \underline{\underline{\Lambda}}\right)^{-1} \left(m_j \underline{g} - \frac{1}{N_j} \underline{\nabla}\left(N_j k T_j\right) + q_j \underline{E}'\right) \tag{23}$$

$$\underline{w_j} = \frac{1}{m_j \nu_{jn}} \left(\underline{\underline{I}} - \kappa_j \underline{\underline{\Lambda}}\right)^{-1} \left(m_j \underline{g} - \frac{1}{N_j} \underline{\nabla}\left(N_j k T_j\right) + q_j \underline{E}'\right) \tag{24}$$

$$\underline{w_j} = \frac{1}{N_j q_j} \left(\underline{Q_j} + \underline{\underline{S_j}}\, \underline{E}'\right) \tag{25}$$

where $\underline{\underline{I}}$ is the identity matrix and κ_j, which has the same sign as q_j, is $q_j B/m_j \nu_{jn}$. $|\kappa_j|$ is the ratio of the gyrofrequency, $|q_j|\, B/m_j$, to the collision frequency, ν_{jn}. $\underline{Q_j}$ and $\underline{\underline{S_j}}$ are:

$$\underline{Q_j} = \frac{N_j q_j}{m_j \nu_{jn}} \left(\underline{\underline{I}} - \kappa_j \underline{\underline{\Lambda}}\right)^{-1} \left(m_j \underline{g} - \frac{1}{N_j} \underline{\nabla}\left(N_j k T_j\right)\right) \tag{26}$$

$$\underline{\underline{S_j}} = \frac{N_j q_j^2}{m_j \nu_{jn}} \left(\underline{\underline{I}} - \kappa_j \underline{\underline{\Lambda}}\right)^{-1} \tag{27}$$

[22] Although $\underline{\underline{\Lambda}}^{-1}$ does not exist, $(\underline{\underline{I}} - \kappa_j\underline{\underline{\Lambda}})^{-1}$ does exist for all $\kappa_j \neq \infty$. Substituting equation (25) into equation (21) gives an expression for $\underline{J}$.

$$\underline{J} = \left(\sum_j \underline{Q_j}\right) + \left(\sum_j \underline{\underline{S_j}}\right)\underline{E'} \tag{28}$$

$$\underline{J} = \underline{Q} + \underline{\underline{S}}\,\underline{E'} \tag{29}$$

where $\underline{Q}$ and $\underline{\underline{S}}$ are:

$$\underline{Q} = \sum_j \frac{N_j q_j}{m_j \nu_{jn}} \left(\underline{\underline{I}} - \kappa_j\underline{\underline{\Lambda}}\right)^{-1} \left(m_j\underline{g} - \frac{1}{N_j}\nabla(N_j k T_j)\right) \tag{30}$$

$$\underline{\underline{S}} = \sum_j \frac{N_j q_j^2}{m_j \nu_{jn}} \left(\underline{\underline{I}} - \kappa_j\underline{\underline{\Lambda}}\right)^{-1} \tag{31}$$

[23] The directions of $\underline{Q_j}$ and $\underline{\underline{S_j}}\,\underline{E'}$ are controlled by κ_j. If $\kappa_j \ll 1$ (weak field), then $\underline{Q_j}$ is parallel to gravitational and pressure gradient forces, which are usually vertical, and $\underline{\underline{S_j}}\,\underline{E'}$ is parallel to $\underline{E'}$. If $\kappa_j \gg 1$ (strong field), then both $\underline{Q_j}$ and $\underline{\underline{S_j}}\,\underline{E'}$ are parallel to $\underline{B}$.

[24] A related relationship between $\underline{J}$ and $\underline{E'}$ is given by *Eccles* [2004]. However, it is not frame-independent, has only one ion species, and neglects the effects of gravity near the magnetic equator (equation (2b) of *Eccles* [2004]). *Eccles* [2004] solves these equations after assuming that the component of the electric field parallel to the magnetic field is zero. This assumption is not consistent with the situation that arises during ambipolar diffusion, either in the weak-field limit or in the limit of strong vertical field (equation (12)).

5. Comparison of $\underline{J} = \underline{Q} + \underline{\underline{S}}\,\underline{E'}$ and $\underline{J} = \underline{\underline{\sigma}}\,\underline{E'}$

[25] The relationship $\underline{J} = \underline{Q} + \underline{\underline{S}}\,\underline{E'}$ is different from the conductivity equation, $\underline{J} = \underline{\underline{\sigma}}\,\underline{E'}$, which is the usual version of Ohm's Law used in ionospheric physics, where $\underline{\underline{\sigma}}$ is the conductivity tensor. $\underline{J} = \underline{\underline{\sigma}}\,\underline{E'}$ is derived from the momentum equations under the assumption that gravitational and pressure gradient forces are negligible [*Forbes*, 1981; *Richmond*, 1983; *Kelley*, 1989]. If gravitational and pressure gradient forces are neglected, does $\underline{J} = \underline{Q} + \underline{\underline{S}}\,\underline{E'}$ reduce to $\underline{J} = \underline{\underline{\sigma}}\,\underline{E'}$? In this case, $\underline{Q} = 0$ and, since $\underline{\underline{S}}$ is independent of gravitational and pressure gradient forces, the question reduces to whether $\underline{\underline{S}}$ equals $\underline{\underline{\sigma}}$ (equations (30) and (31)).

[26] $\underline{J} = \underline{\underline{\sigma}}\,\underline{E'}$, a frame-independent equation, is derived from the frame-independent momentum equations. However, ionospheric physics textbooks do not give a frame-independent representation of the conductivity tensor, which suggests that the powerful tools of linear algebra are not being fully utilized in the derivation and application of $\underline{J} = \underline{\underline{\sigma}}\,\underline{E'}$. In order to compare $\underline{\underline{S}}$ and $\underline{\underline{\sigma}}$, we assume that $\underline{B} = B\,\hat{\underline{z}}$. Using equation (19),

$$\left(\underline{\underline{I}} - \kappa_j\underline{\underline{\Lambda}}\right)^{-1} = \begin{pmatrix} 1 & -\kappa_j & 0 \\ \kappa_j & 1 & 0 \\ 0 & 0 & 1 \end{pmatrix}^{-1} \tag{32}$$

$$\left(\underline{\underline{I}} - \kappa_j\underline{\underline{\Lambda}}\right)^{-1} = \begin{pmatrix} \frac{1}{\left(1+\kappa_j^2\right)} & \frac{\kappa_j}{\left(1+\kappa_j^2\right)} & 0 \\ \frac{-\kappa_j}{\left(1+\kappa_j^2\right)} & \frac{1}{\left(1+\kappa_j^2\right)} & 0 \\ 0 & 0 & 1 \end{pmatrix} \tag{33}$$

which leads to (equation (31)):

$$\underline{\underline{S}} = \sum_j \frac{N_j q_j^2}{m_j \nu_{jn}} \begin{pmatrix} \frac{1}{\left(1+\kappa_j^2\right)} & \frac{\kappa_j}{\left(1+\kappa_j^2\right)} & 0 \\ \frac{-\kappa_j}{\left(1+\kappa_j^2\right)} & \frac{1}{\left(1+\kappa_j^2\right)} & 0 \\ 0 & 0 & 1 \end{pmatrix} \tag{34}$$

[27] Equation (34) is the usual representation of the conductivity tensor, so $\underline{J} = \underline{Q} + \underline{\underline{S}}\,\underline{E'}$ does reduce to the well-known expression $\underline{J} = \underline{\underline{\sigma}}\,\underline{E'}$ when gravitational and pressure gradient forces are neglected [*Forbes*, 1981; *Richmond*, 1983; *Kelley*, 1989]. $\underline{J} = \underline{\underline{\sigma}}\,\underline{E'}$ is therefore a restricted special case of the more general expression $\underline{J} = \underline{Q} + \underline{\underline{S}}\,\underline{E'}$. Given the widespread use of $\underline{J} = \underline{\underline{\sigma}}\,\underline{E'}$ in ionospheric and magnetospheric physics, $\underline{J} = \underline{Q} + \underline{\underline{S}}\,\underline{E'}$ may have many practical applications. For example, the usual equations of magnetohydrodynamics are derived from $\underline{J} = \underline{\underline{\sigma}}\,\underline{E'}$ [*Gombosi*, 1998]. *Strangeway and Raeder* [2001] discuss the effects of pressure gradients and gravity on collisionless and collisional magnetohydrodynamics. The Earth's ionosphere includes a global layer of metallic ions derived from meteoroids. The ion densities in this layer are strongly affected by the transport of ions due to neutral winds, electric fields, and magnetic fields [*Fesen et al.*, 1983; *Bedey and Watkins*, 1997; *Carter and Forbes*, 1999]. This work may have applications to models of this metallic ion layer.

[28] The *xy* and *yx* elements of $\underline{\underline{S}}$ represent the Hall conductivity, σ_H, the *xx* and *yy* elements represent the Pederson conductivity, σ_P, and the *zz* element represents the direct conductivity, σ_0. If $\kappa_j \rightarrow 0$, then $\sigma_P = \sigma_0$ and $\sigma_H = 0$. If $\kappa_j \rightarrow \infty$, then $\sigma_P = 0$ and $\sigma_H = 0$. Equations (32)–(34) illustrate the close relationship between σ_P and σ_H. The inverse of $\begin{pmatrix} 1 & -\kappa_j \\ \kappa_j & 1 \end{pmatrix}$, which is $\frac{1}{1+\kappa_j^2}\begin{pmatrix} 1 & \kappa_j \\ -\kappa_j & 1 \end{pmatrix}$, has only two distinct elements. The diagonal elements of this inverse matrix contribute to the Pederson conductivity and the off-diagonal elements contribute to the Hall conductivity.

6. Conservation of Charge and Maxwell's Equations

[29] $\underline{B}$, $\underline{E}$, and $\underline{J}$ must conserve charge and satisfy Maxwell's equations. For a quasi-neutral ionosphere, charge conservation becomes:

$$\underline{\nabla} \cdot \underline{J} = 0 \tag{35}$$

[30] Neglecting the effects of planetary rotation and requiring steady state electric and magnetic fields, three of Maxwell's four equations are [*Richmond*, 1983]:

$$\underline{\nabla} \cdot \underline{B} = 0 \tag{36}$$

$$\underline{\nabla} \times \underline{E} = 0 \tag{37}$$

$$\underline{\nabla} \times \underline{B} = \mu_0 \, \underline{J} \tag{38}$$

where μ_0 is the permeability of free space. The missing Maxwell's equation, Gauss's Law, has been replaced by the quasi-neutrality equation, equation (17). The total magnetic field, $\underline{B}$, is expressed as $\underline{B_p} + \underline{B_i}$. One part of the magnetic field, $\underline{B_p}$, is generated by currents flowing within the planet. Above the planetary surface, $\underline{B_p}$ is a known field that satisfies $\underline{\nabla} \cdot \underline{B_p} = 0$ and $\underline{\nabla} \times \underline{B_p} = 0$. $\underline{B_p}$ can be zero. The other part, $\underline{B_i}$, is generated by currents flowing within the ionosphere. $\underline{B_i}$ satisfies $\underline{\nabla} \cdot \underline{B_i} = 0$ and $\underline{\nabla} \times \underline{B_i} = \mu_0 \, \underline{J}$. $\underline{B_i}$ is zero if $\underline{J} = 0$.

7. Ambipolar Diffusion Revisited

[31] The relationship $\underline{J} = \underline{Q} + \underline{\underline{S}} \, \underline{E'}$ raises the possibility of current flowing in the absence of an electric field or an electric field existing without causing a current to flow, if $\underline{\nabla} \times \underline{E} = 0$, $\underline{\nabla} \cdot \underline{J} = 0$, and the appropriate boundary conditions are satisfied. Ambipolar diffusion, a common model for ionospheric plasma transport, occurs when $\underline{J} = 0$ but not all $\underline{w_j}$ are zero. If we assume that $\underline{J} = 0$, which automatically satisfies $\underline{\nabla} \cdot \underline{J} = 0$, then equations (25) and (29) lead to:

$$\underline{E'} = -\underline{\underline{S}}^{-1} \underline{Q} \tag{39}$$

$$N_j q_j \underline{w_j} = \underline{Q_j} - \underline{\underline{S_j}} \underline{\underline{S}}^{-1} \underline{Q} \tag{40}$$

[32] Is this consistent with known results for ambipolar diffusion in the absence of a magnetic field (equation (11))? We first assume that $m_e \nu_{en} \ll m_i \nu_{in}$, that $\nu_{en} \ll \nu_{in}$, and that there is only one species of ion, labeled i, whereas electrons are labeled e, so $N_i = N_e = N$ [*Rishbeth and Garriott*, 1969; *Banks and Kockarts*, 1973]. Since $\underline{J}$ is zero, $\underline{w_i} = \underline{w_e} = \underline{w}$. We use equations (30)–(31), set $\kappa_j = 0$ since $B = 0$, and neglect some small terms to find that:

$$\underline{Q} = \left(\frac{Ne}{m_i \nu_{in}} \right) m_i \underline{g} + \frac{e}{m_e \nu_{en}} \underline{\nabla}(NkT_e) \tag{41}$$

$$\underline{\underline{S}} = \frac{Ne^2}{m_e \nu_{en}} \underline{\underline{I}} \tag{42}$$

[33] Using the ion version of equation (40) and equations (41)–(42), $\underline{w}$ satisfies:

$$\begin{aligned} Ne\underline{w} = {} & \frac{Ne}{m_i \nu_{in}} \left(m_i \underline{g} - \frac{1}{N} \underline{\nabla}(NkT_i) \right) \\ & - \left(\frac{Ne^2}{m_i \nu_{in}} \right) \left(\frac{m_e \nu_{en}}{Ne^2} \right) \left(\frac{Ne}{m_i \nu_{in}} m_i \underline{g} + \frac{e}{m_e \nu_{en}} \underline{\nabla}(NkT_e) \right) \end{aligned} \tag{43}$$

[34] Rearranging,

$$Ne\underline{w} = \left(\frac{Ne}{m_i \nu_{in}} \right) m_i \underline{g} \left(1 - \frac{m_e \nu_{en}}{m_i \nu_{in}} \right) - \frac{e}{m_i \nu_{in}} \underline{\nabla}(Nk(T_i + T_e)) \tag{44}$$

[35] Neglecting a small term ($m_e \nu_{en} \ll m_i \nu_{in}$) and rearranging again,

$$\underline{w} = \frac{1}{m_i \nu_{in}} \left(m_i \underline{g} - \frac{1}{N} \underline{\nabla}(Nk(T_i + T_e)) \right) \tag{45}$$

which is consistent with earlier results (equation (11)) [*Rishbeth and Garriott*, 1969].

8. Dynamo Equation

[36] Equation (37) can be rewritten as:

$$\underline{E} = -\underline{\nabla} \phi \tag{46}$$

where ϕ is a scalar potential. Equations (16), (29), (35), and (46) can be combined to obtain:

$$\underline{\nabla} \cdot \left(\underline{Q} + B \underline{\underline{S}} \, \underline{\underline{\Lambda}} \, \underline{u} - \underline{\underline{S}} \, \underline{\nabla} \phi \right) = 0 \tag{47}$$

[37] Equation 47, a second-order partial differential equation in ϕ with variable coefficients, is an extension of the "dynamo equation" [*Forbes*, 1981]. If the dynamo equation can be solved for ϕ, then the unknowns $\underline{E}$, $\underline{E'}$, $\underline{J}$, $\underline{w_j}$, $\underline{v_j}$, and $\underline{B_i}$ can be determined straight-forwardly.

[38] One approach to solving equation (47) is as follows. If all the variables in equation (47), except ϕ, are known throughout the volume of interest then equation (47) can be rewritten as:

$$\begin{aligned} 0 = {} & \alpha + \beta_r E_r + \beta_\theta E_\theta + \beta_\phi E_\phi + \gamma_{rr} \frac{\partial E_r}{\partial r} + \gamma_{r\theta} \frac{\partial E_r}{\partial \theta} + \gamma_{r\phi} \frac{\partial E_r}{\partial \phi} \\ & + \gamma_{\theta r} \frac{\partial E_\theta}{\partial r} + \gamma_{\theta\theta} \frac{\partial E_\theta}{\partial \theta} + \gamma_{\theta\phi} \frac{\partial E_\theta}{\partial \phi} + \gamma_{\phi r} \frac{\partial E_\phi}{\partial r} + \gamma_{\phi\theta} \frac{\partial E_\phi}{\partial \theta} \\ & + \gamma_{\phi\phi} \frac{\partial E_\phi}{\partial \phi} \end{aligned} \tag{48}$$

where the α, β and γ coefficients are known throughout the volume of interest. Suppose that the volume of interest has a spherical lower boundary ($r = R$) on which $\underline{E}$ is specified. Six of the nine partial derivatives of $\underline{E}$ that appear in equation (48), those with respect to θ and ϕ, are therefore known at $r = R$. $\frac{\partial E_\theta}{\partial r}$ and $\frac{\partial E_\phi}{\partial r}$ can be found at $r = R$ from equation (37) ($\underline{\nabla} \times \underline{E} = 0$). The remaining partial derivative, $\frac{\partial E_r}{\partial r}$, can be found at $r = R$ using equation (48). Since $\underline{E}$ and all its first-order partial derivatives are known at $r = R$, $\underline{E}$ at $r = R + \Delta r$ can be found. This can be extended outwards until $\underline{E}$ is known throughout the volume of interest.

[39] The choice of a spherical polar coordinate frame and spherical lower boundary is convenient, but not necessary. This technique can be applied as long as either $\underline{E}$ or $\underline{J}$ is specified on a continuous surface that separates the system

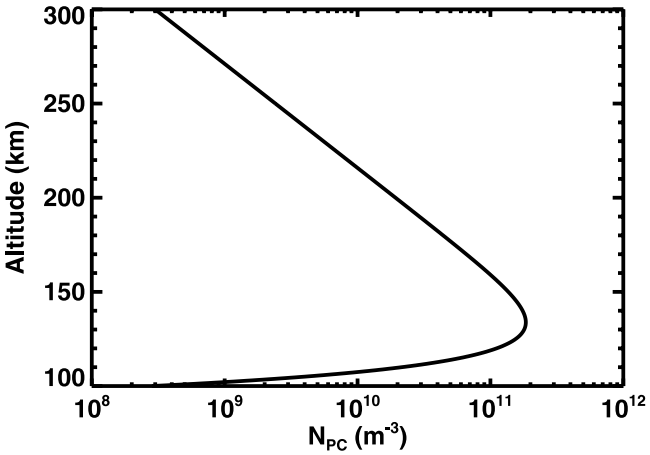

Figure 1. Vertical profile of electron density (N_{PC}) for simulation PC.

into two parts. If $\underline{J}$ is specified on the boundary, $\underline{E}$ can be found on that boundary using equations (16) and (29).

9. One-Dimensional Ionospheric Model

[40] Sections 1–8 have derived a frame-independent relationship between $\underline{J}$ and $\underline{E}$ that includes the three-dimensional effects of gravity and pressure gradients. This relationship can be used in an ionospheric model to make testable predictions about a planetary ionosphere. Those predictions may differ from predictions made by other models. In this initial paper, we use this relationship in a one-dimensional ionospheric model. It will be applied to two-dimensional and three-dimensional models in future work.

[41] We assume that B and $\underline{\underline{\Lambda}}$ are independent of $\underline{B_i}$. If $\underline{B_i}$ is strong enough to affect the velocity of ions and electrons, the plasma dynamics are beyond the scope of this paper. Ionospheric models are commonly used to determine unknown properties $\underline{E}(z)$, $\underline{J}(z)$, $\underline{v_i}(z)$, and $\underline{B_i}(z)$ from known properties $N_j(z)$, $T_j(z)$, q_j, m_j, $\nu_{jn}(z)$, $\underline{u}(z)$, and $\underline{B_P}(z)$, where z is altitude. Results for $\underline{v_i}(z)$ can then be used to model how $N_j(z)$ changes with time. With this assumption, $\underline{Q}$ and $\underline{\underline{S}}$ are functions of the known properties.

[42] Since $\underline{J} = \underline{Q} + \underline{\underline{S}}\,\underline{E'}$ and $\underline{E'} = \underline{E} + B\underline{\underline{\Lambda}}\,\underline{u}$ (equations (29) and (16), respectively), $\underline{J}$ satisfies:

$$\underline{J} = \underline{R} + \underline{\underline{S}}\,\underline{E} \tag{49}$$

where $\underline{R} = \underline{Q} + B\underline{\underline{S}}\,\underline{\underline{\Lambda}}\,\underline{u}$ is a function of the known properties. The z component of equation (49) is:

$$J_z = R_z + S_{zx}E_x + S_{zy}E_y + S_{zz}E_z \tag{50}$$

[43] Suppose that the ionosphere has no horizontal gradients. Since $\underline{\nabla} \times \underline{E} = 0$, $\partial E_x/\partial z$ and $\partial E_y/\partial z$ are zero, so E_x and E_y are uniform. $\underline{\nabla} \cdot \underline{J} = 0$ becomes $\partial J_z/\partial z = 0$, so J_z is also uniform. Suppose that either $\underline{E}$ or $\underline{J}$ is specified on the lower or upper boundary of the ionosphere. The other vector (either $\underline{J}$ or $\underline{E}$) can be determined at that altitude using equation (49). Now that E_x, E_y, and J_z, which are all uniform, are all specified on the boundary, E_z can be determined at any altitude from equation (50) using $\underline{R}$ and $\underline{\underline{S}}$, which are known:

$$E_z = \frac{J_z}{S_{zz}} - \frac{R_z}{S_{zz}} - \frac{S_{zx}}{S_{zz}}E_x - \frac{S_{zy}}{S_{zz}}E_y \tag{51}$$

[44] Thus $\underline{E}$ can be determined at all altitudes. $\underline{E'}$ follows from equation (16), $\underline{J}$ follows from equation (29), $\underline{w_i}$ follows from equation (25), and $\underline{v_i}$ follows from equation (15). For this one-dimensional case, $\underline{B_i}$ satisfies (equation (38)).

$$\frac{\partial B_{i,x}}{\partial z} = \mu_0\, J_y \tag{52}$$

$$\frac{\partial B_{i,y}}{\partial z} = -\mu_0\, J_x \tag{53}$$

$$\frac{\partial B_{i,z}}{\partial z} = 0 \tag{54}$$

[45] Equations (52)–(54) can be used to find $\underline{B_i}$ at all altitudes, given a boundary condition for $\underline{B_i}$. $\underline{J} = 0$ and $\underline{B_i} = 0$ are plausible lower boundary conditions for a one-dimensional ionospheric model, provided the altitude of the lower boundary is chosen appropriately.

10. Application to Mars-Like One-Dimensional Ionosphere

[46] In this section, we apply the theory of section 9 to an idealized one-dimensional ionospheric model. Our main purpose is to convincingly demonstrate that the formalism developed in this paper leads to self-consistent ion velocities, electron velocities, currents, and electric fields, especially through the dynamo region. Existing models do not do so. We anticipate that application of this formalism to current systems in the martian ionosphere will be interesting, given the non-dipolar, non-global martian magnetic field and the small number of previous studies of martian ionospheric currents. The secondary purpose of this section is to make predictions concerning currents in the martian ionosphere and so the model is designed to reflect some, but not all, of the properties of the martian ionosphere [*Withers et al.*, 2005]. This is discussed in more detail in section 10.1. An important point is that this model is not intended to make accurate predictions of $N_j(z)$ far above the main peak.

[47] The continuity equation for species j is [*Rishbeth and Garriott*, 1969]:

$$\frac{\partial N_j}{\partial t} + \underline{\nabla} \cdot \left(N_j \underline{v_j}\right) = P_j - L_j \tag{55}$$

where P_j and L_j are the rates of production and loss of species j, respectively. Preceding sections of this paper obtained steady state solutions for $\underline{v_j}$. A scale analysis indicates that changes in $\underline{v_j}$ are much faster than changes in N_j, so steady state solutions for $\underline{v_j}$ can be used to simulate how N_j varies with time [*Richmond*, 1983].

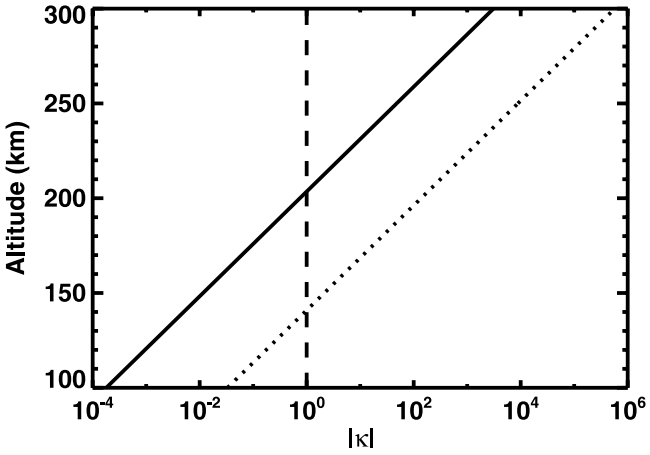

Figure 2. $|\kappa_e|$ (dotted line) and $|\kappa_i|$ (solid line) for all simulations. $|\kappa| = 1$ is marked by the dashed line.

[48] In section 10, we develop a photochemical-only version of the model that does not include transport processes (section 10.1), use the photochemical-only results to determine what $\underline{v_j}$ and related properties would be if transport processes were suddenly "switched on" (section 10.2), conduct sensitivity studies (section 10.3), and allow transport processes to bring N_j to steady state (section 10.4).

10.1. Model Details

[49] The neutral atmosphere is assumed to be composed of CO_2 with a uniform scale height of 12 km and a number density of 1.4×10^{12} cm^{-3} at 100 km [*Fox et al.*, 1996]. Gravity is 3.7 m s^{-2}, the flux of ionizing photons at 1 AU is 5×10^{10} cm^{-2} s^{-1}, the planet is at 1.5 AU from the Sun, and the Sun is directly overhead [*Martinis et al.*, 2003; *Withers and Mendillo*, 2005]. CO_2 molecules have an absorption cross-section of 10^{-17} cm^2 [*Schunk and Nagy*, 2000] and, adopting a simplified photochemistry, each photon that is absorbed results in the immediate creation of a single O_2^+ ion [*Chamberlain and Hunten*, 1987; *Fox et al.*, 1996]. The ionosphere is quasi-neutral and there is only one species of ions, so $N_i = N_e$. Ions are lost by dissociative recombination with electrons; this process has a dissociative recombination coefficient, α_{DR}, of 2×10^{-7} cm^3 s^{-1} [*Schunk and Nagy*, 2000]. In the absence of transport processes, these assumptions mean that the ionosphere has the shape of an alpha-Chapman layer, as shown in Figure 1 [*Chapman*, 1931a, 1931b; *Rishbeth and Garriott*, 1969]. We label these photochemical-only plasma densities as N_{PC}. The maximum electron number density, 2×10^{11} m^{-3}, occurs at 134 km.

[50] Ion-neutral and electron-neutral collision frequencies are calculated as follows [*Banks and Kockarts*, 1973]:

$$\nu_{jn} = 2.9 \times 10^{-9} \frac{m_n}{m_j + m_n} n_n \sqrt{\frac{\alpha_{pol}}{m_r}} \tag{56}$$

where ν_{jn} is in units of s^{-1}, n_n is in units of cm^{-3}, α_{pol} is in units of 10^{-24} cm^3, m_r is in units of daltons, m_n is the mass of the neutral species, n_n is the number density of the neutral species, α_{pol} is the polarizability of the neutral species, and m_r is the reduced mass of the charged and neutral species. α_{pol} for CO_2 is 2.911×10^{-24} cm^3 [*Lide*, 1994].

[51] The magnetic field strength is assumed to be uniform, 50 nT. Its direction is specified for each simulation in turn (sections 10.2–10.4). The base of the dynamo region occurs where $\nu_{en} = \Omega_e$, 141 km. The top of the dynamo region occurs where $\nu_{in} = \Omega_i$, 204 km. The center of the dynamo region is around 170 km. The ratio of gyrofrequency to collision frequency, $|\kappa|$, is shown in Figure 2. $|\kappa_e/\kappa_i| = 184$. The wind speed, $\underline{u}$, is assumed to be zero and the model's altitude range is 100–300 km. Lower boundary conditions are $\underline{J} = 0$ and $\underline{B_i} = 0$, so $v_{i,z} = v_{e,z} = v_z$.

[52] The model's chemistry is realistic around the main peak generated by solar EUV photons. It cannot reproduce the lower ionospheric layer that is generated by solar X-rays due to its monochromatic solar spectrum [*Fox et al.*, 1996; *Mendillo et al.*, 2006]. It cannot simulate observed plasma densities above about 200 km due to its neglect of O^+ ions [*Chen et al.*, 1978]. Therefore simulated electron densities and currents should be realistic around the main peak and in the dynamo region. Simulated topside electron densities and velocities will not match observations at high altitudes.

10.2. Solution for Plasma Velocity and Related Properties

[53] We now perform one simulation, called simulation PC, using the inputs and assumptions of section 10.1. The goal is to calculate what $\underline{v_i}$ and $\underline{v_e}$ would be if transport processes were suddenly "switched on" in the photochemical-only ionosphere. $\underline{B} = B\,(\hat{\underline{x}} + \hat{\underline{z}})/\sqrt{2}$. As $\underline{B}$ is inclined at 45° to the horizontal, $I = 45°$. We use the results of section 9 to find $\underline{v_i}$, $\underline{v_e}$, $\underline{B_i}$, $\underline{J}$, and $\underline{E}$ starting from $N_i = N_e = N_{PC}$. Results for v_z are shown in Figure 3. Also shown in Figure 3 are $v_{ambi,weak}$ and $v_{ambi,strong}$, the weak field and strong field limits of ambipolar diffusion.

$$v_{ambi,weak} = \frac{-(m_i + m_e)g}{m_i \nu_{in} + m_e \nu_{en}} \left(1 + \frac{2kT}{(m_i + m_e)g} \frac{\partial \ln N}{\partial z}\right) \tag{57}$$

$$v_{ambi,strong} = v_{ambi,weak} \times \sin^2 I \tag{58}$$

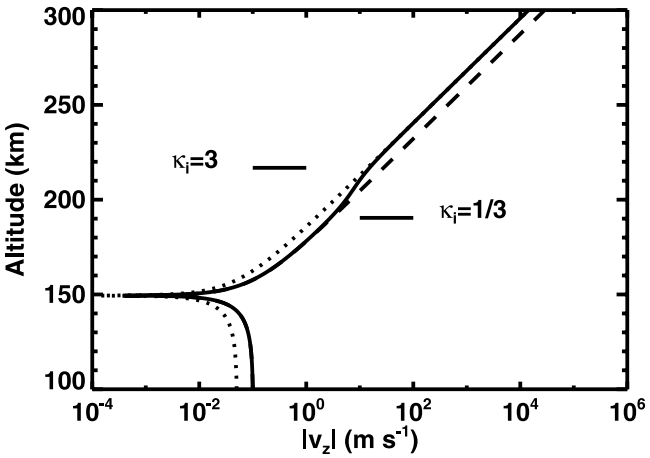

Figure 3. v_z (solid line), $v_{ambi,weak}$ (dashed line), and $v_{ambi,strong}$ (dotted line) for simulation PC. v_z, $v_{ambi,weak}$, and $v_{ambi,strong}$ are negative below 150 km and positive above 150 km. $v_z = v_{ambi,weak}$ at low altitudes and $v_z = v_{ambi,strong}$ at high altitudes.

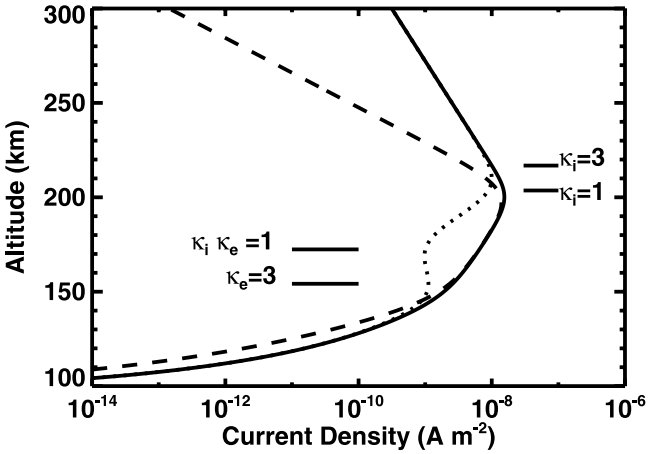

Figure 4. $-J_x$ (dashed line), J_y (dotted line), and $|J|$ (solid line) for simulation PC. $J_z = 0$.

[54] Equation (57) is derived from equation (10). Equation (57) reduces to equation (11) and equation (45) if small terms are neglected. v_z transitions from $v_{ambi,weak}$ at low altitudes to $v_{ambi,strong}$ at high altitudes, and the altitude of the transition region is controlled by κ_i, not κ_e. Results for $\underline{J}$ are shown in Figure 4. $|J| \geq 10\%$ of its maximum value between 148 and 262 km, which extends above the dynamo region. E_z is -1.3×10^{-5} V m^{-1} at the lower boundary, increases monotonically with increasing altitude, passes through 0 at 134 km, and approaches 8.5×10^{-7} V m^{-1} at higher altitudes. $B_{i,x}$ and $B_{i,y}$, which are both positive at all altitudes above the lower boundary and increase monotonically with altitude, are less than 1 nT. $B_i \ll B_p$, as was assumed. In order to study how tightly ions and electrons are frozen in to fieldlines, we define θ_j as follows:

$$\cos(\theta_j) = \frac{\underline{v_j} \cdot \underline{\hat{b}}}{\left|\underline{v_j}\right|} \tag{59}$$

[55] Figure 5 shows θ_i and θ_e. $\theta_j = 0°$ corresponds to motion parallel to $\underline{B}$ and $\theta_j = 180°$ corresponds to motion antiparallel to $\underline{B}$. For $\underline{B} = B\,(\underline{\hat{x}} + \underline{\hat{z}})/\sqrt{2}$, $\theta_j = 45°$ corresponds to upward motion and $\theta_j = 135°$ corresponds to downward motion. At low altitudes, neither ions nor electrons are tied to magnetic fieldlines (θ_i, θ_e = 45° or 135°). At high altitudes, both ions and electrons are tied to magnetic fieldlines (θ_i, θ_e = 0° or 180°). At intermediate altitudes, electrons, but not ions, are tied to magnetic fieldlines (θ_e = 0°, θ_i = 45°).

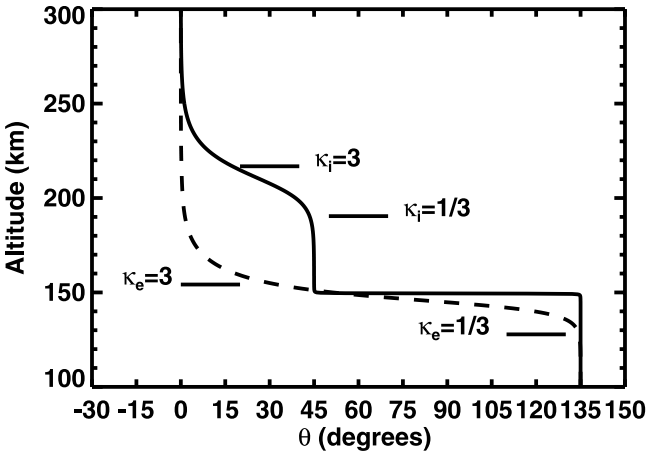

Figure 5. θ_e (dashed line) and θ_i (solid line) for simulation PC. θ_e and θ_i change from the weak field limit to the strong field limit at altitudes where $\kappa_e = 1$ and $\kappa_i = 1$, respectively.

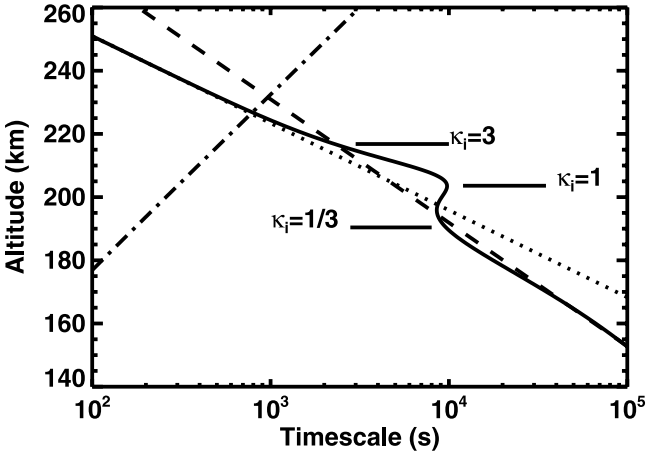

Figure 6. τ_{trans} (solid line) and τ_{PC} (dot-dash line) for simulation PC. τ_{trans} follows one trend at low altitude (dashed line) and another at high altitude (dotted line).

[56] Figures 3 and 5 confirm that both ion and electron velocities transition smoothly between the expected limits of the weak and the strong cases. Neither ambipolar diffusion nor the usual conductivity equation, $\underline{J} = \underline{\underline{\sigma}}\,\underline{E}$, can accomplish this. Results for $\underline{E}$, $\underline{J}$, $\underline{v_i}$, $\underline{v_e}$, and $\underline{B_i}$ are smooth and self-consistent.

[57] Figure 6 shows the timescales for photochemical loss, τ_{PC}, and for transport processes, τ_{trans}. $\tau_{PC} = 1/\alpha_{DR}N$ and τ_{trans} is defined by [*Rishbeth and Garriott*, 1969]:

$$\frac{N}{\tau_{trans}} = \left|\frac{\partial}{\partial z}(Nv_z)\right| \tag{60}$$

[58] Photochemical loss occurs faster than gain or loss of ions/electrons by transport below 227 km. Figure 6 shows how the transport timescale follows one trend below $\kappa_i = 1/3$ and a different trend above $\kappa_i = 3$. This occurs because $v_z \simeq v_{ambi,weak}$ below $\kappa_i = 1/3$ and $v_z \simeq v_{ambi,strong}$ above $\kappa_i = 3$, where $v_{ambi,strong} = v_{ambi,weak}/2$.

10.3. Sensitivity Studies

[59] Results of section 10.2 for $\underline{E}$, $\underline{J}$, $\underline{v_i}$, and $\underline{v_e}$ are obtained from the solution of algebraic, not differential, equations, so they are insensitive to the number of altitude levels used. Only the results for $\underline{B_i}$ involve the integration of a differential equation. Boundary conditions are applied at the lower boundary only, so the results are insensitive to the altitude of the upper boundary. However, the results might be sensitive to the altitude of the lower boundary. We performed sensitivity studies by moving the lower boundary from 100 km to 120 km and 80 km.

[60] E_z changed by less than 2×10^{-10} V m^{-1}. v_z changed by less than 0.1%, except for a narrow region

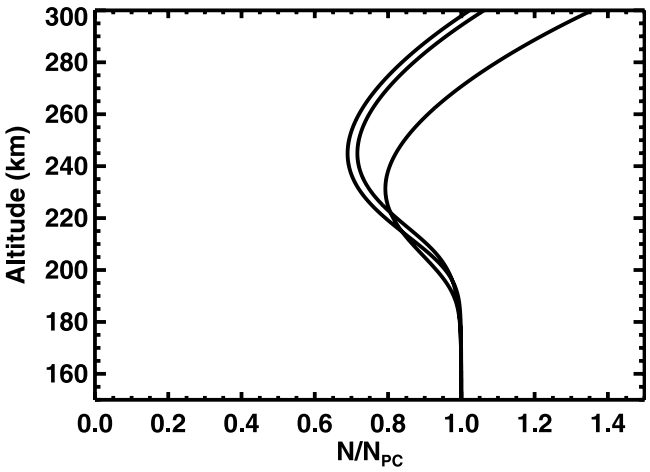

Figure 7. Three N/N_{PC} profiles for simulations 1.1–1.3. The value of N at 300 km in simulation 1.3 ($v_z = v_{ambi,strong}$) is less than in simulation 1.1 (v_z from section 9), which is less than in simulation 1.2 ($v_z = v_{ambi,weak}$).

where $v_{i,z}$ passes through zero. J_x and J_y changed by more than 10% below 150 km and by less than 1% above 175 km. $B_{i,x}$ and $B_{i,y}$ changed by more than 10% below 160 km and by less than 1% above 220 km. E_z and v_z are insensitive to changes in the altitude of the lower boundary, but $\underline{J}$ and $\underline{B_i}$ are not.

10.4. Steady State Solution

[61] Sections 10.1 to 10.3 have shown how the results of section 9 affect plasma velocities, fields, and currents in a Chapman-like ionosphere with only photochemical processes. We now allow transport processes to change plasma densities from the photochemical-only values (N_{PC}), aiming for steady state solutions. Equation (55) requires a boundary condition

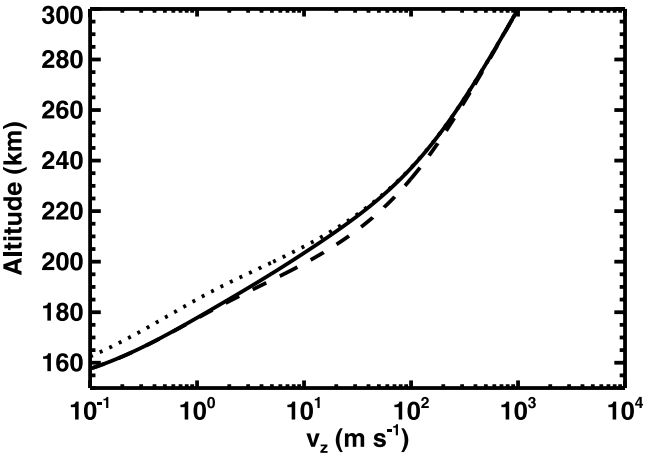

Figure 8. Results for v_z for simulations 1.1–1.3. v_z in simulations 1.1 (solid line, v_z from section 9) and 1.2 (dashed line, $v_z = v_{ambi,weak}$) are similar at low altitudes, below the dynamo region. v_z in simulations 1.1 (solid line, v_z from section 9) and 1.3 (dotted line, $v_z = v_{ambi,strong}$) are similar at high altitudes, above the dynamo region. The same upper boundary condition, $v_z = 1000$ m s^{-1}, was used in all three simulations.

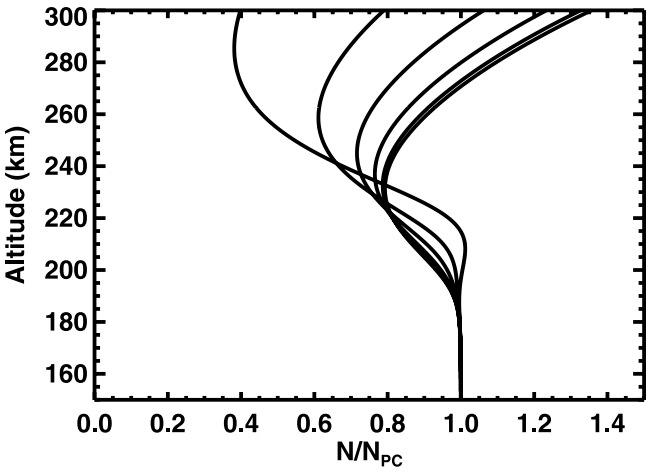

Figure 9. Six N/N_{PC} profiles for simulations 2.1–2.6. N at 300 km increases as I increases.

for v_z, so we assume that $v_z = 1000$ m s^{-1} at the upper boundary [*Chen et al.*, 1978]. Results are sensitive to this boundary condition. This speed may seem high, but *Chen et al.* [1978] found that high speeds were required to reproduce Viking observations of high altitude plasma densities, especially O^+ and H^+. Similar upper boundary conditions are used in the most comprehensive model of the martian ionosphere [*Fox*, 1997; *Fox and Yeager*, 2006].

[62] Two sets of simulations, labeled 1 and 2, were performed. In set 1, three simulations were performed using the inputs and assumptions in section 10.1, so I remained at 45°. Simulation 1.1 used the results of section 9 to find v_z. Simulation 1.2 used ambipolar diffusion velocities in the weak-field limit, $v_z = v_{ambi,weak}$ (equation (57)). Simulation 1.3 used ambipolar diffusion velocities in the strong-field limit, $v_z = v_{ambi,strong}$ (equation (58)). Results are shown in Figures 7–8. Steady state $N(z)$ and $v_z(z)$ for simulation 1.1 differ significantly from the results of simulations 1.2 and 1.3.

[63] In set 2, six simulations were performed using the inputs and assumptions in section 10.1. The results of

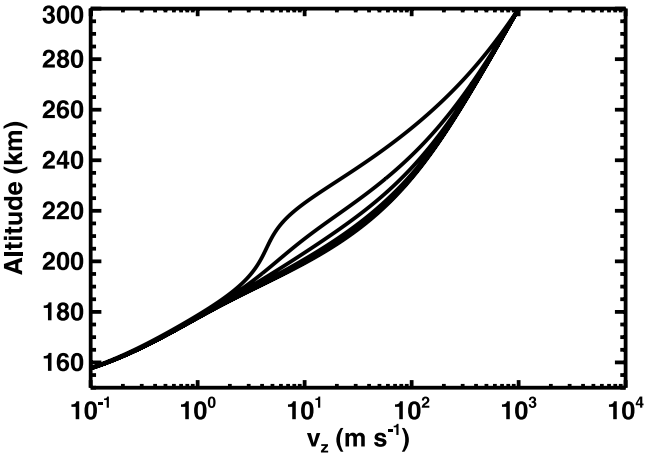

Figure 10. Results for v_z for simulations 2.1–2.6. v_z at 240 km increases as I increases. The same upper boundary condition, $v_z = 1000$ m s^{-1}, was used in all six simulations.

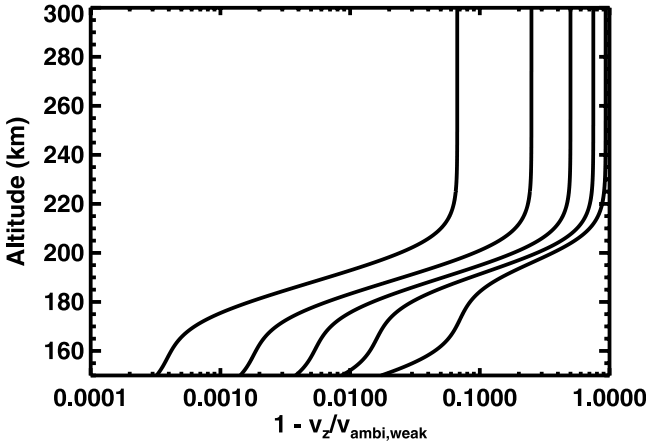

Figure 11. Results for v_z for simulations 2.1–2.6. $1 - v_z/v_{ambi,weak}$ decreases as I increases. $v_z = v_{ambi,weak}$ and $1 - v_z/v_{ambi,weak} = 0$ for $I = 90°$ (simulation 2.6).

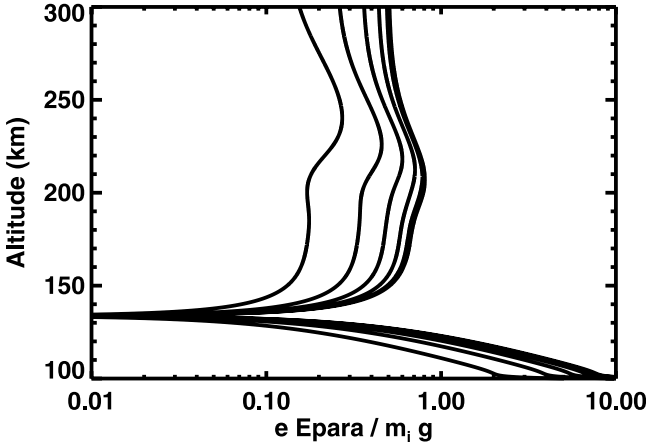

Figure 13. Results for E_{para} for simulations 2.1–2.6. E_{para} increases as I increases.

section 9 were used to find v_z. Six magnetic field inclinations above the horizontal were used, 15°, 30°, 45°, 60°, 75°, and 90°, corresponding to simulations 2.1–2.6, respectively. $I = 90°$ (simulation 2.6) corresponds to a vertical field, which is effectively the same as zero field. Magnetic field magnitude remained 50 nT.

[64] Results are shown in Figures 9 –14. N varies by tens of percent depending on field inclination (Figure 9). v_z varies by almost an order of magnitude depending on field inclination (Figure 10). $|J|$ varies by an order of magnitude for $I = 15°$ to $I = 75°$ (Figure 12). $|J|$ is zero for $I = 90°$. The magnitude of the electric field parallel to $\underline{B}$, E_{para}, is given by $|\underline{E} \cdot \hat{\underline{b}}|$ and the magnitude of the electric field perpendicular to $\underline{B}$, E_{perp}, is given by $|\underline{E} - (\underline{E} \cdot \hat{\underline{b}})\,\hat{\underline{b}}|$ (Figures 13–14). The effects of these electric fields on ions are comparable in magnitude to the effects of gravity throughout the dynamo region.

[65] These results may be compared to recent observations of the martian ionosphere by a topside radar sounder, MARSIS, on the Mars Express spacecraft [*Nielsen et al.*, 2006]. In these observations, electron densities at 200 km generally exceed those predicted with a photochemical Chapman-like model. Measurement uncertainties are not stated. By contrast, electron densities in Figure 9 are similar to a photochemical Chapman-like model at 200 km and are smaller than the model at 220–240 km. There are several possible explanations for this difference, including the absence of O^+ from this work and the plasma velocity of 1 km s^{-1} assumed as an upper boundary condition in this work. O^+, an atomic ion, has a longer lifetime than O_2^+, a molecular ion. Thus an increased proportion of O^+ ions could cause greater-than-expected electron densities, as seen in the terrestrial F-layer. However, two Viking lander Retarding Potential Analyzer (RPA) measurements did not show a high enough proportion of O^+ to explain the observations of *Nielsen et al.* [2006] [*Hanson et al.*, 1977]. The implications of the Viking RPA data should not be over-stated because this pair of observations is insufficient to constrain how the O^+/O_2^+ ratio varies with local time, season, latitude and solar activity. Theoretical models of the neutral atmosphere predict large variations in the O/CO_2 ratio that imply large variations in the O^+/O_2^+

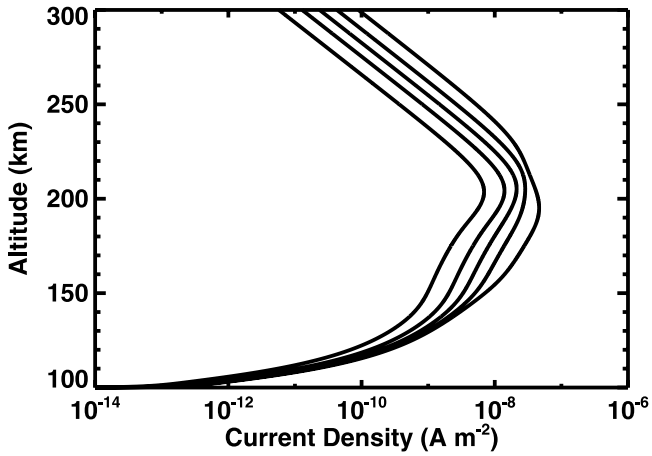

Figure 12. Results for $|J|$ for simulations 2.1–2.6. $|J|$ decreases as I increases. $|J| = 0$ for $I = 90°$ (simulation 2.6).

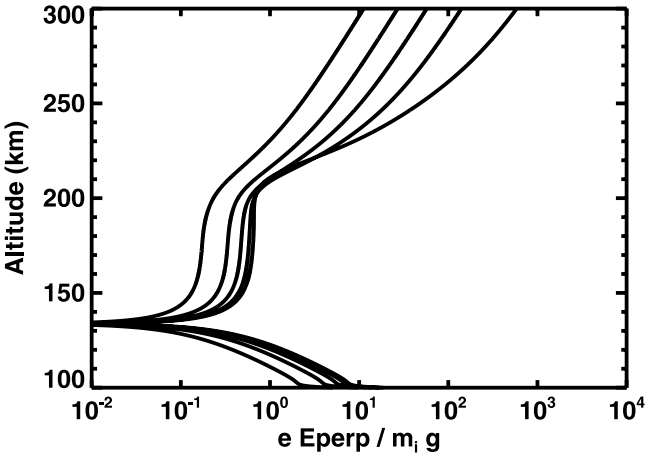

Figure 14. Results for E_{perp} for simulations 2.1–2.6. E_{perp} at 180 km and 240 km decreases as I increases. $E_{perp} = 0$ for $I = 90°$ (simulation 2.6).

ratio [*Bougher et al.*, 1999, 2000]. Additional observations of ion composition are required to definitively determine the importance of O^+ in the topside martian ionosphere. Alternatively, reducing the upward plasma velocity on the upper boundary would make Figure 9 more similar to the observations of *Nielsen et al.* [2006]. The large upward velocity of 1 km s^{-1} is required in one-dimensional models that reproduce the Viking RPA data [*Chen et al.*, 1978]. Three-dimensional models can use a combination of horizontal motion and slower vertical motion to reproduce these observations. Unfortunately, there are no direct observations of plasma velocity in the martian ionosphere to constrain such models.

11. Conclusions

[66] Existing theory offers an incomplete description of ionospheric electrodynamics and plasma transport. $\underline{J} = \underline{\underline{\sigma}}\,\underline{E}'$ neglects pressure gradients and gravitational forces, whereas ambipolar diffusion, which assumes that $\underline{J} = 0$, breaks down within a dynamo region. A more general relationship exists between currents and electric fields in an ionosphere: $\underline{J} = \underline{Q} + \underline{\underline{S}}\,\underline{E}'$. Expressions for $\underline{Q}$ and $\underline{\underline{S}}$ have been derived assuming that collisions between charged particles can be neglected. $\underline{J} = \underline{Q} + \underline{\underline{S}}\,\underline{E}'$ reduces to $\underline{J} = \underline{\underline{\sigma}}\,\underline{E}'$ when pressure gradients and gravitational forces are neglected. $\underline{J} = \underline{Q} + \underline{\underline{S}}\,\underline{E}'$ reduces to the equations governing ambipolar diffusion if $\underline{J}$ is set equal to zero. A ''dynamo equation,'' a second order partial differential equation in ϕ, the scalar electric potential, has also been derived from $\underline{J} = \underline{Q} + \underline{\underline{S}}\,\underline{E}'$. Models based on these equations will be able to generate self-consistent descriptions of currents, ion velocities, electron velocities, and electric fields.

[67] A one-dimensional ionospheric model that uses $\underline{J} = \underline{Q} + \underline{\underline{S}}\,\underline{E}'$ has been developed and used to find steady state plasma densities and velocities. The results show ion and electron velocities transitioning smoothly from one limiting case (weak field) at low altitudes to another limiting case (strong field) at high altitudes. This corresponds to charged particles being frozen-in to fieldlines at high, but not low, altitudes. The main purpose of the model is a demonstration of that transition, not reproduction of any specific observations. However, since the model is a simplistic representation of the martian ionosphere, it has been used to predict current densities in the martian ionosphere as a function of inclination for a 50 nT field and zero wind. Current densities on the order of 10^{-8} A m^{-2} were predicted. Because of the neglect of O^+ ions in the model, simulated electron densities should not be compared to martian observations above about 200 km.

[68] Many sophisticated models of the terrestrial ionosphere, such as TIE-GCM, MTIE-GCM, CTIP, and CMIT, use the incomplete relationship $\underline{J} = \underline{\underline{\sigma}}\,\underline{E}'$ to determine ionospheric electrodynamics [*Richmond et al.*, 1992; *Peymirat et al.*, 1998; *Millward et al.*, 2001; *Wang et al.*, 2004]. Others assume that the electric field is determined by the electron pressure gradient [*Ridley et al.*, 2006]. Some predictions of such models might be different if $\underline{J} = \underline{Q} + \underline{\underline{S}}\,\underline{E}'$ was used instead.

[69] **Acknowledgments.** The author acknowledges useful discussions with Michael Mendillo and other colleagues in the Center for Space Physics. The author also acknowledges two anonymous reviewers. This project was initiated using support from NSF's CEDAR Postdoctoral Research Program.

[70] Wolfgang Baumjohann thanks Stephan Buchert and Joseph Huba for their assistance in evaluating this paper.

References

Acuña, M. H., et al. (1999), Global distribution of crustal magnetization discovered by the Mars Global Surveyor MAG/ER experiment, *Science*, *284*, 790–793.

Banks, P. M., and G. Kockarts (1973), *Aeronomy*, Elsevier, New York.

Bedey, D. F., and B. J. Watkins (1997), Large-scale transport of metallic ions and the occurrence of thin ion layers in the polar ionosphere, *J. Geophys. Res.*, *102*(A5), 9675–9681.

Bougher, S. W., S. Engel, R. G. Roble, and B. Foster (1999), Comparative terrestrial planet thermospheres: 2. Solar cycle variation of global structure and winds at equinox, *J. Geophys. Res.*, *104*(E7), 16,591–16,611.

Bougher, S. W., S. Engel, R. G. Roble, and B. Foster (2000), Comparative terrestrial planet thermospheres: 3. Solar cycle variation of global structure and winds at solstices, *J. Geophys. Res.*, *105*(E7), 17,669–17,692.

Carter, L. N., and J. M. Forbes (1999), Global transport and localized layering of metallic ions in the upper atmosphere, *Ann. Geophys.*, *17*, 190–209.

Chamberlain, J. W., and D. M. Hunten (1987), *Theory of Planetary Atmospheres*, 2nd ed., Elsevier, New York.

Chandra, S. (1964), Plasma diffusion in the ionosphere, *J. Atmos. Sol. Terr. Phys.*, *26*, 113–122.

Chapman, S. (1931a), The absorption and dissociative or ionizing effect of monochromatic radiation in an atmosphere on a rotating Earth, *Proc. Phys. Soc.*, *43*, 26–45.

Chapman, S. (1931b), The absorption and dissociative or ionizing effect of monochromatic radiation in an atmosphere on a rotating Earth. Part II: Grazing incidence, *Proc. Phys. Soc.*, *43*, 483–501.

Chen, R. H., T. E. Cravens, and A. F. Nagy (1978), The Martian ionosphere in light of the Viking observations, *J. Geophys. Res.*, *83*(A8), 3871–3876.

Connerney, J. E. P., M. H. Acuña, P. J. Wasilewski, N. F. Ness, H. Reme, C. Mazelle, D. Vignes, R. P. Lin, D. L. Mitchell, and P. A. Cloutier (1999), Magnetic lineations in the ancient crust of Mars, *Science*, *284*, 794–798.

Eccles, J. V. (2004), The effect of gravity and pressure in the electrodynamics of the low-latitude ionosphere, *J. Geophys. Res.*, *109*, A05304, doi:10.1029/2003JA010023.

Fesen, C. G., P. B. Hays, and D. N. Anderson (1983), Theoretical modeling of low-latitude Mg, *J. Geophys. Res.*, *88*(A4), 3211–3223.

Forbes, J. M. (1981), The equatorial electrojet, *Rev. Geophys. Space Phys.*, *19*, 469–504.

Fox, J. L. (1997), Upper limits to the outflow of ions at Mars: Implications for atmospheric evolution, *Geophys. Res. Lett.*, *24*(22), 2901–2904.

Fox, J. L., and K. E. Yeager (2006), Morphology of the near-terminator Martian ionosphere: A comparison of models and data, *J. Geophys. Res.*, *111*, A10309, doi:10.1029/2006JA011697.

Fox, J. L., P. Zhou, and S. W. Bougher (1996), The Martian thermosphere/ionosphere at high and low solar activities, *Adv. Space Res.*, *17*, 203–218.

Gombosi, T. I. (1998), *Physics of the Space Environment*, Cambridge Univ. Press, New York.

Hanson, W. B., S. Sanatani, and D. R. Zuccaro (1977), The Martian ionosphere as observed by the Viking retarding potential analyzers, *J. Geophys. Res.*, *82*(28), 4351–4363.

Kelley, M. (1989), *The Earth's Ionosphere*, Elsevier, New York.

Lide, D. R. (1994), *CRC Handbook of Chemistry and Physics*, 75th ed., CRC Press, Boca Raton, Fla.

Martinis, C. R., J. K. Wilson, and M. J. Mendillo (2003), Modeling day-to-day ionospheric variability on Mars, *J. Geophys. Res.*, *108*(A10), 1383, doi:10.1029/2003JA009973.

Mendillo, M., P. Withers, D. Hinson, H. Rishbeth, and B. Reinisch (2006), Effects of solar flares on the ionosphere of Mars, *Science*, *311*, 1135–1138, doi:10.1126/science.1122099.

Millward, G. H., I. C. F. Müller-Wodarg, A. D. Aylward, T. J. Fuller-Rowell, A. D. Richmond, and R. J. Moffett (2001), An investigation into the influence of tidal forcing on F region equatorial vertical ion drift using a global ionosphere-thermosphere model with coupled electrodynamics, *J. Geophys. Res.*, *106*(A11), 24,733–24,744.

Nielsen, E., H. Zou, D. A. Gurnett, D. L. Kirchner, D. D. Morgan, R. Huff, R. Orosei, A. Safaeinili, J. J. Plaut, and G. Picardi (2006), Observations of vertical reflections from the topside Martian ionosphere, *Space Sci. Rev.*, *126*, 373–388, doi:10.1007/s11214-006-9113-y.

Peymirat, C., A. D. Richmond, B. A. Emery, and R. G. Roble (1998), A magnetosphere-thermosphere-ionosphere electrodynamics general circulation model, *J. Geophys. Res.*, *103*(A8), 17,467–17,477.

Richmond, A. D. (1983), Thermospheric dynamics and electrodynamics, in *Solar-Terrestrial Physics*, edited by R. L. Carovillano and J. M. Forbes, pp. 523–608, Springer, New York.

Richmond, A. D., M. Blanc, P. Amayenc, B. A. Emery, R. H. Wand, B. G. Fejer, R. F. Woodman, S. Ganguly, R. A. Behnke, and C. Calderon (1980), An empirical model of quiet-day ionospheric electric fields at middle and low latitudes, *J. Geophys. Res.*, *85*(A9), 4658–4664.

Richmond, A. D., E. C. Ridley, and R. G. Roble (1992), A thermosphere/ionosphere general circulation model with coupled electrodynamics, *Geophys. Res. Lett.*, *19*(6), 601–604.

Ridley, A. J., Y. Deng, and G. Tóth (2006), The global ionosphere thermosphere model, *J. Atmos. Sol. Terr. Phys.*, *68*, 839–864, doi:10.1016/j.jastp.2006.01.008.

Rishbeth, H. (1997), The ionospheric E-layer and F-layer dynamos — A tutorial review, *J. Atmos. Sol. Terr. Phys.*, *59*, 1873–1880.

Rishbeth, H., and O. K. Garriott (1969), *Introduction to Ionospheric Physics*, Elsevier, New York.

Schunk, R. W., and A. F. Nagy (2000), *Ionospheres*, chap. 4, Cambridge Univ. Press, New York.

Strangeway, R. J., and J. Raeder (2001), On the transition from collisionless to collisional magnetohydrodynamics, *J. Geophys. Res.*, *106*(A2), 1955–1960.

Wang, W., M. Wiltberger, A. G. Burns, S. C. Solomon, T. L. Killeen, N. Maruyama, and J. G. Lyon (2004), Initial results from the coupled magnetosphere-ionosphere-thermosphere model: Thermosphere-ionosphere responses, *J. Atmos. Sol. Terr. Phys.*, *66*, 1425–1441, doi:10.1016/j.jastp.2004.04.008.

Withers, P., and M. Mendillo (2005), Response of peak electron densities in the Martian ionosphere to day-to-day changes in solar flux due to solar rotation, *Planet. Space Sci.*, *53*, 1401–1418, doi:10.1016/j.pss.2005.07.010.

Withers, P., M. Mendillo, H. Rishbeth, D. P. Hinson, and J. Arkani-Hamed (2005), Ionospheric characteristics above Martian crustal magnetic anomalies, *Geophys. Res. Lett.*, *32*, L16204, doi:10.1029/2005GL023483.

P. Withers, Center for Space Physics, Boston University, 725 Commonwealth Avenue, Boston, MA 02215, USA. (withers@bu.edu)